INTERLIBRARY LOAN

The WSU Libraries' goal is to provide excellent customer service. Let us know how we are doing by responding to this short survey:
https://libraries.wsu.edu/access_services_survey

JOURNAL OF GUIDANCE, CONTROL, AND DYNAMICS
Vol. 41, No. 11, November 2018

Engineering Notes

Three-Axis Attitude Determination Using Magnetorquers

Danil Ivanov,* Mikhail Ovchinnikov,† and Dmitry Roldugin‡
Keldysh Institute of Applied Mathematics, Russian Academy of Sciences, 125047 Moscow, Russia

DOI: 10.2514/1.G003698

I. Introduction

ACTIVE magnetic attitude control system is the most common for micro- and nanosatellites in low Earth orbit. It is used for the angular velocity damping, stabilization along the geomagnetic induction vector, spin stabilization, and even three-axis attitude acquisition. Proper stabilization requires the real-time determination of the attitude motion. It is obtained by processing the attitude sensors' measurements. Sun sensors [1], magnetometers [2,3], angular velocity sensors [4,5], and even micro star tracker [6,7] are commonly used for the attitude motion determination. However, the tendency for miniaturization and simplification leads to the requirements of control systems with a minimal set of hardware. For example, three-axis attitude control is available with the sole magnetometer and three magnetorquers for a CubeSat [8,9]. Note that commercial off-the-shelf sensors are prone to faults, and small satellites rarely benefit from any backup measures. Thus, there is a high risk of early mission loss because of the magnetometer failure. However, it is still possible to determine the angular motion using measurements of the induced electromotive force (EMF) in magnetorquers.

This paper considers the satellite equipped with the solenoid magnetorquers (i.e., coils wound into a tightly packed helix). The magnetic flux enclosed by the nonoperating coil is changing due to the angular motion in the geomagnetic field. According to the well-known Faraday's law, this causes the induced EMF in magnetorquers. It may be measured by the analog-to-digital converter and then processed by the extended Kalman filter. The attitude state vector estimation is available during the uncontrolled motion of the satellite. Afterward, the necessary control torque may be implemented using the same magnetorquers. The proposed scheme at the least could provide a back-up solution in case of attitude sensor malfunction.

Magnetorquers act like the three-axis induction coil sensor during the passive attitude motion. In [10], a review of such sensor constructions and applications is presented. These sensors are commonly used to measure the magnetic flux variation frequency or detect the altering magnetic fields. The magnetic field induction value can be calculated by the integration of the output signal from the coils. However, unknown zero voltage offset poses a problem. Measurements of the magnetorquers that are proportional to the magnetic flux derivative should be used for the attitude motion determination.

The extended Kalman filter is used for the attitude state vector estimation [11]. The measurements model of the induced EMF takes into account the attitude, angular velocity, and variation of the geomagnetic field along the orbit. The attitude motion model includes the dynamic and kinematic equations; the attitude is represented by the quaternion. This paper studies the accuracy of the proposed algorithm and its dependence on the measurements noise. Three-axis magnetic control acting in conjunction with the proposed attitude determination scheme is considered.

II. Attitude Motion Equations

Rigid spacecraft angular motion is considered. The satellite is equipped with three mutually orthogonal magnetorquers. Two reference frames are used, defined as follows.

$OX_1X_2X_3$ is the orbital reference frame located at the satellite center of mass. OX_3 is directed along the satellite radius vector, OX_1 is directed along the orbital velocity, and OX_2 is directed so that the reference frame is right-handed.

$Ox_1x_2x_3$ is the body reference frame; its axes coincide with the principal axes of inertia of the satellite.

Satellite attitude is represented with different parameters. Euler angles α, β, γ (rotation sequence 1-2-3) are used for the convenient representation of results and control construction. The direction cosines matrix $\boldsymbol{A}$ and its elements a_{ij} are used in control construction. The quaternion $\Lambda = (\boldsymbol{q}, q_0)$ is used for the numerical simulation and Kalman filter construction. Angular velocity may represent either the absolute motion ($\boldsymbol{\omega}$ and its components ω_i) or relative motion with respect to the orbital reference frame ($\boldsymbol{\Omega}$ and Ω_i). The absolute and relative velocities are related by

$$\boldsymbol{\omega} = \boldsymbol{\Omega} + \boldsymbol{A}\boldsymbol{\omega}_{\text{orb}}$$

where $\boldsymbol{\omega}_{\text{orb}} = (0, \omega_0, 0)$ is the orbital reference frame angular velocity for the circular orbit. Euler equations for the satellite with inertia tensor $\boldsymbol{J} = \text{diag}(A, B, C)$ are

$$\boldsymbol{J}\dot{\boldsymbol{\omega}} + \boldsymbol{\omega} \times \boldsymbol{J}\boldsymbol{\omega} = \boldsymbol{M}$$

The torque $\boldsymbol{M}$ may contain the control part $\boldsymbol{M}_{\text{ctrl}}$ and the disturbing part. The latter is divided into the gravitational $\boldsymbol{M}_{\text{gr}}$ and the unknown one $\boldsymbol{M}_{\text{dist}}$, so that overall $\boldsymbol{M} = \boldsymbol{M}_{\text{ctrl}} + \boldsymbol{M}_{\text{gr}} + \boldsymbol{M}_{\text{dist}}$. The control torque is

$$\boldsymbol{M}_{\text{ctrl}} = \boldsymbol{m} \times \boldsymbol{B}$$

where $\boldsymbol{m}$ is the dipole control moment of the satellite, and $\boldsymbol{B}$ is the geomagnetic induction vector in the bound reference frame. Gravitational torque is

$$\boldsymbol{M}_{\text{gr}} = 3\omega_0^2(\boldsymbol{A}\boldsymbol{e}_3) \times \boldsymbol{J}(\boldsymbol{A}\boldsymbol{e}_3)$$

where $\boldsymbol{e}_3 = (0, 0, 1)$ is the satellite radius vector in the orbital frame. Disturbing torque $\boldsymbol{M}_{\text{dist}}$ is modeled as a random noise with Gaussian distribution of the order of $5 \cdot 10^{-8}$ N · m. Because the numerical modeling is provided for the 400 km altitude, the main source of the disturbance is the atmospheric drag. The torque value is given by

Received 20 March 2018; revision received 1 June 2018; accepted for publication 12 July 2018; published online 17 September 2018.

*Senior Researcher, Attitude Control and Guidance Division; danilivanovs@gmail.com.

†Head of Division, Attitude Control and Guidance Division; ovchinni@keldysh.ru. Senior Member AIAA.

‡Senior Researcher, Attitude Control and Guidance Division; rolduginds@gmail.com.

$$M_{\text{aero}} = \frac{1}{2}\rho S c_x v^2 \Delta$$

Assume that the atmosphere density is $\rho = 4 \cdot 10^{-12}$ kg/m^3 for mean solar activity according to CIRA-2012; the average 1U CubeSat without any external panels or antennas area is $S = 10^{-2}$ m^2; the drag coefficient $c_x = 2$; and the displacement between the center of mass and the center of pressure is $\Delta = 0.5$ cm. This provides the typical atmospheric drag torque to be about $7 \cdot 10^{-9}$ N $\cdot$ m. Increasing this by a magnitude is a general measure to accommodate some specific factors such as large solar panels (increasing both the area and the displacement of the center of pressure) or peak solar activity.

The dynamical equation for the relative motion is

$$\boldsymbol{J}\dot{\boldsymbol{\Omega}} = \boldsymbol{M} + \boldsymbol{M}_{\text{gir}} + \boldsymbol{J}\boldsymbol{\Omega} \times \boldsymbol{A}\boldsymbol{\omega}_{\text{orb}} \tag{1}$$

where $\boldsymbol{M}_{\text{gir}} = -\boldsymbol{\omega} \times \boldsymbol{J}\boldsymbol{\omega}$ is the gyroscopic torque.

Dynamical equations are supplemented with the kinematic relations. Quaternion kinematics is

$$\dot{\boldsymbol{q}} = \frac{1}{2}(q_0\boldsymbol{\Omega} + \boldsymbol{W}_{\Omega}\boldsymbol{q}), \quad \dot{q}_0 = -\frac{1}{2}\boldsymbol{q}^T\boldsymbol{\Omega} \tag{2}$$

where $\boldsymbol{W}_y$ is a skew-symmetric matrix for any vector $\boldsymbol{y}$:

$$\boldsymbol{W}_y = \begin{pmatrix} 0 & y_3 & -y_2 \\ -y_3 & 0 & y_1 \\ y_2 & -y_1 & 0 \end{pmatrix}$$

The inclined dipole model is mainly used to represent the geomagnetic field [12]. It allows quite accurate field representation [13] paired with simple computational procedures. The geomagnetic induction vector is

$$\boldsymbol{B} = \frac{\mu_e}{r^5}(\boldsymbol{k}r^2 - 3(\boldsymbol{k}\boldsymbol{r})\boldsymbol{r})$$

where $\boldsymbol{k}$ is the Earth's dipole unit vector, $\boldsymbol{r}$ is the satellite radius vector, r is the satellite radius vector magnitude, and $\mu_e = 7.812 \cdot 10^6$ km$^3 \cdot$ kg $\cdot$ s$^{-2} \cdot$ A^{-1}. The direct dipole model ($\boldsymbol{k}$ is antiparallel to the Earth rotation axis) is used for analytical approaches; the geomagnetic induction vector in the orbital frame in this model is

$$\boldsymbol{B}_{\text{orb}} = B_0 \begin{pmatrix} \cos u \sin i \\ \cos i \\ -2 \sin u \sin i \end{pmatrix} \tag{3}$$

where $B_0 = \mu_e/r^3$, u is the argument of latitude, and i is the orbit inclination.

III. Magnetorquers Measurement Model

A. CubeSats Magnetorquers Typical Parameters

Magnetic coils, also referred to as magnetorquers, are especially valuable for CubeSat-class nanosatellites. They are commercially available in two typical configurations: in loose coils of flat wound wire, and in tightly wound coils around a permalloy rod. The rod configuration is preferable because of high permeability of the core material. Consider the rod-type magnetorquers developed at the Department of Earth and Space Science and Engineering, York University [14]. Its core diameter is 5.7 mm, the number of turns is 6063, the maximum magnetic dipole is 0.3 A $\cdot$ m^2, and hysteresis rod relative permeability is about 75,000.

Another type of magnetorquer is made of flat wire coils or manufactured in electronic layers. These are often called the air core magnetorquers. Flat coils are conveniently placed inside CubeSats. Consider CUTE-1.7+APD II magnetorquers in the orthogonal configuration [15] as an example. Each magnetorquer has dimensions $58.5 \times 78.3 \times 1.6$ mm^3 with 3000 wire turns. The maximum magnetic dipole is 0.15 A $\cdot$ m^2. Both magnetorquer configurations are often combined in one ready-to-use board. Such a board is used, for example, in Delfi-n3Xt CubeSat. It consists of a set of two x- and y-axis magnetorquer rods and one z-axis air core magnetorquer.

B. Measurement Model

Consider the CubeSat with three orthogonal magnetorquer coils. The attitude motion is passive (e.g., the magnetorquers do not produce any commanded control moment). Because the satellite rotates in the geomagnetic field, an EMF V is induced in the coil according to Faraday's law:

$$V_i = -N\frac{d\Phi_i}{dt} = -NS\frac{d(\boldsymbol{B}, \boldsymbol{n}_i)}{dt}, \qquad i = x, y, z \tag{4}$$

where Φ is the magnetic flux passing through the coil with the area S an with a number of turns N, and $\boldsymbol{n}_i$ are normal vectors to the coils planes. Assume that vectors $\boldsymbol{n}_i$ are directed along the satellite reference frame axes. Then, Eq. (4) can be rewritten as

$$\boldsymbol{V} = -NS\frac{d\boldsymbol{B}}{dt}$$

In case of the magnetorquer rods, it is necessary to take into account the auxiliary magnetic field $\boldsymbol{H}$ inside the rod material. It is related to the geomagnetic field $\boldsymbol{B}$ as

$$\boldsymbol{B} = \mu\boldsymbol{H}$$

where μ is the core permeability. Ferromagnetic core strengthens the external magnetic field in the coil and increases the output signal:

$$\boldsymbol{V} = -NS\mu\frac{d\boldsymbol{H}}{dt}$$

That is why, despite the small coil area of the magnetorquer rod compared to the air core coil, its EMF may be larger due to the large value of μ (about $10^5\mu_0$, where μ_0 is the magnetic constant). However, the relative permeability of the core μ_c may be much lower than the material permeability [16]. This is due to the demagnetizing field effect expressed by the geometry-dependent demagnetizing factor D:

$$\mu_c = \frac{\mu_r}{1 + D(\mu_r - 1)}$$

where $\mu_r = \mu/\mu_0$.

To use the EMF measurements in the attitude determination process, it is necessary to convert the analog signal V into the digital value. Thus, the control system should include the analog-to-digital converter (ADC). The most critical feature of ADC is its sensitivity. If the reference signal of the ADC is 1 V, then the 16 bit converter has a resolution of about 15 μV [17]. This is the minimum value that can be theoretically detected. However, the ADC is subjected to errors due to the thermal noise in electrical circuit, errors in temperature bias, etc. At best, the errors do not exceed 2 bit signal values. That is why digital measures are noisy, and the final measurement model is

$$\boldsymbol{V} = -NS\frac{d\boldsymbol{B}}{dt} + \boldsymbol{\eta}_V \tag{5}$$

where $\boldsymbol{\eta}_V$ is the noise that is considered to be normally distributed. Note that some nonrandom errors may arise due to local onboard nonstationary magnetic fields. However, the EMF measurements are based on the derivative of the magnetic field induction vector. This eliminates the majority of the nonrandom noise. Also, the hysteresis effects in the magnetorquer core may also complicate the measurements, although in the Earth magnetic field, the hysteresis rods will be far away from saturation. Thus, this effect is negligible.

The magnetorquer is a solenoid with the inductance L, and the latter be estimated by the formula

$$L = \frac{\mu_0 N^2 S}{l}$$

where l is the length of the coil. It affects the change in the current I:

$$I = I_0 e^{-t/\tau}$$

where I_0 is the coil current, $\tau = L/R$ is the relaxation time, and R is the resistance of the coil. For the CubeSat, typical magnetorquers τ does not exceed several milliseconds. Thus, if the sampling time dT between the measurements is more than τ, delays in the measurements have a small effect.

IV. Extended Kalman Filter Application

A. Kalman Filter Basics

The extended Kalman filter (EKF) is a well-known and well-established algorithm. It is characterized by the relatively small computational cost and provides the estimation of the state vector that is not directly measured.

The Kalman filter is a recursive algorithm that uses the dynamical system model and sensor readings for the actual motion determination. The state vector estimation $\hat{\boldsymbol{x}}_{k-1}^{+} = \hat{\boldsymbol{x}}(t_k)$ is calculated for each discrete time step t_k when the measurements are available. The discrete Kalman filter uses the correction of the previous estimate [18]. Consider step $k-1$ along with the corresponding state vector estimation $\hat{\boldsymbol{x}}_{k-1}^{+}$ and covariance matrix $\boldsymbol{P}_{k-1}^{+}$. The goal is to find the state vector estimation for the next step $\hat{\boldsymbol{x}}_{k}^{+}$. First, the a priori estimate $\hat{\boldsymbol{x}}_{k}^{-}$ is formed using straight mathematical model integration. It is corrected using the sensor measurements vector $\boldsymbol{z}_k$ to obtain the a posteriori estimate $\hat{\boldsymbol{x}}_{k}^{+}$. The covariance error matrix $\boldsymbol{P}_{k}^{-}$ is also constructed from the previous step information using Riccati equation. It is then updated to $\boldsymbol{P}_{k}^{+}$ using measurements.

The Kalman filter is designed for linear mathematical models and allows the best mean-square state vector estimation. However, it may be extended for any nonlinear mathematical models of both the dynamical system and the measurements:

$$\dot{\boldsymbol{x}}(t) = \boldsymbol{f}(\boldsymbol{x}, t) + \boldsymbol{G}\boldsymbol{w}(t),$$
$$\dot{\boldsymbol{z}}(t) = \boldsymbol{h}(\boldsymbol{x}, t) + \boldsymbol{v}(t)$$

where $\boldsymbol{w}(t)$ is the Gaussian dynamical model error with the covariance matrix $\boldsymbol{D}$, $\boldsymbol{G}$ is the matrix of influence of the model error on the state vector, and $\boldsymbol{v}(t)$ is the Gaussian measurements error with the covariance matrix $\boldsymbol{R}$.

EKF requires the decomposition of the right-side functions $\boldsymbol{f}(\boldsymbol{x}, t)$ and $\boldsymbol{h}(\boldsymbol{x}, t)$ into the Taylor series in the vicinity of the current state vector. Only linear terms are used in the filter. The dynamical system matrix $\boldsymbol{F}$ and measurements model $\boldsymbol{H}$ matrix are

$$\boldsymbol{F}_k = \left.\frac{\partial \boldsymbol{f}(\boldsymbol{x}, t)}{\partial \boldsymbol{x}}\right|_{\boldsymbol{x}=\hat{\boldsymbol{x}}_k^-, t=t_k}, \qquad \boldsymbol{H}_k = \left.\frac{\partial \boldsymbol{h}(\boldsymbol{x}, t)}{\partial \boldsymbol{x}}\right|_{\boldsymbol{x}=\hat{\boldsymbol{x}}_k^-, t=t_k}$$

The discrete EKF uses the nonlinear dynamical and measurements models for a priori estimate prediction and a posteriori correction [19]. The prediction phase is

$$\hat{\boldsymbol{x}}_{k}^{-} = \int_{t_{k-1}}^{t_k} \boldsymbol{f}(\boldsymbol{x}, t)\,\mathrm{d}t,$$
$$\boldsymbol{P}_{k}^{-} = \boldsymbol{\Phi}_k \boldsymbol{P}_{k-1}^{+} \boldsymbol{\Phi}_k^T + \boldsymbol{Q}_k$$

where $\boldsymbol{Q}_k$ is the covariance matrix of the discrete-time process noise; it is calculated as

$$\boldsymbol{Q}_k = \int_{t_{k-1}}^{t_k} \boldsymbol{\Phi}_k \boldsymbol{G}\boldsymbol{D}\boldsymbol{G}^T \boldsymbol{\Phi}_k^T\,\mathrm{d}t \tag{6}$$

The correction phase is

$$\boldsymbol{K}_k = \boldsymbol{P}_k^{-}\boldsymbol{H}_k^T(\boldsymbol{H}_k\boldsymbol{P}_k^{-}\boldsymbol{H}_k^T + \boldsymbol{R}_k)^{-1},$$
$$\hat{\boldsymbol{x}}_k^{+} = \hat{\boldsymbol{x}}_k^{-} + \boldsymbol{K}_k(z_k - \boldsymbol{h}(\hat{\boldsymbol{x}}_k^{-}, t_k)),$$
$$\boldsymbol{P}_k^{+} = (\boldsymbol{E} - \boldsymbol{K}_k\boldsymbol{H}_k)\boldsymbol{P}_k^{-}$$

where $\boldsymbol{\Phi}_k = \exp(\boldsymbol{F}_k(t_k - t_{k-1}))$ is the transition matrix between the states $k-1$ and k; $\boldsymbol{E}$ is an identity matrix; and $\boldsymbol{K}$ is the weighing matrix.

B. Equations Linearization

The EKF to obtain the satellite attitude in the orbital reference frame should be constructed. The state vector is

$$\boldsymbol{x} = (\boldsymbol{q}, \Omega)$$

The dynamical model of the controlled satellite angular motion is presented by Eq. (1), and quaternion kinematic equation as in Eq. (2) is used. Equations of motion should be linearized in the vicinity of the current state vector. Rewrite Eqs. (1) and (2) as

$$\delta\dot{\boldsymbol{x}}(t) = \boldsymbol{F}(t)\delta\boldsymbol{x}(t)$$

where $\delta\boldsymbol{x}(t)$ is a small state vector increment, and $\boldsymbol{F}(t)$ is the matrix of the equations of motion linearized in the vicinity of the current state. The state vector $\boldsymbol{x}(t)$ can be divided into the estimated part $\hat{\boldsymbol{x}}(t)$ and the misalignment $\delta\boldsymbol{x}(t)$:

$$\boldsymbol{x}(t) = \hat{\boldsymbol{x}}(t) + \delta\boldsymbol{x}(t)$$

To linearize Eqs. (1) and (2), note that the quaternion sum actually means the sum of rotations. This is represented by the quaternion multiplication in Rodrigues–Hamilton parameters:

$$\Lambda = \hat{\Lambda} \circ \delta\Lambda$$

Here, $\hat{\Lambda}$ is the current estimated quaternion, and $\delta\Lambda$ is the quaternion representing a small rotation. Suppose that $\delta\Lambda = (\delta\boldsymbol{q}, 1)$. This allows an approximate expression

$$\boldsymbol{A}(\delta\Lambda) = \boldsymbol{E} - 2\boldsymbol{W}_{\delta q}$$

Using these assumptions, the obtained dynamics matrix $\boldsymbol{F}$ is

$$\boldsymbol{F} = \begin{pmatrix} -\boldsymbol{W}_{\Omega} & \frac{1}{2}\boldsymbol{E} \\ \boldsymbol{J}^{-1}(6\omega_0^2\boldsymbol{F}_{\mathrm{gr}} + \boldsymbol{F}_{\mathrm{gir}}^{q} + 2\boldsymbol{W}_{J\Omega}\boldsymbol{W}_{A\omega_{\mathrm{orb}}} + 2\boldsymbol{W}_m\boldsymbol{W}_{\hat{B}}) & \boldsymbol{J}^{-1}(\boldsymbol{F}_{\mathrm{gir}}^{\Omega} - \boldsymbol{W}_{A\omega_{\mathrm{orb}}}\boldsymbol{J}) \end{pmatrix}$$

where

$$\boldsymbol{F}_{\mathrm{gr}} = \boldsymbol{W}_{Ae_3}\boldsymbol{J}\boldsymbol{W}_{Ae_3} - \boldsymbol{W}_{JAe_3}\boldsymbol{W}_{Ae_3},$$
$$\boldsymbol{F}_{\mathrm{gir}}^{\Omega} = \boldsymbol{W}_{J\Omega} - \boldsymbol{W}_{\Omega}\boldsymbol{J},$$
$$\boldsymbol{F}_{\mathrm{gir}}^{q} = 2(\boldsymbol{W}_{J\omega}\boldsymbol{W}_{A\omega_{\mathrm{orb}}} - \boldsymbol{W}_{\omega}\boldsymbol{J}\boldsymbol{W}_{A\omega_{\mathrm{orb}}})$$

Using the relation $\boldsymbol{B} = \boldsymbol{A}\boldsymbol{B}_{\mathrm{orb}}$, the magnetorquer measurements in model Eq. (5) can be rewritten as

$$z = -NS\frac{d(\boldsymbol{A}\boldsymbol{B}_{\text{orb}})}{dt} + \boldsymbol{\eta}_V = -NS[-\boldsymbol{\Omega}\times\boldsymbol{B} + \boldsymbol{A}(\boldsymbol{\omega}_0\times\boldsymbol{B}_{\text{orb}})] + \boldsymbol{\eta}_V$$

where $\boldsymbol{\eta}_V$ is a Gaussian geomagnetic induction vector error with zero mean. The measurements matrix after the linearization is as follows:

$$\boldsymbol{H} = -NS[-2\boldsymbol{W}_{\Omega}\boldsymbol{W}_{\hat{B}} - 2\boldsymbol{W}_{A\dot{B}_{\text{orb}}}\boldsymbol{W}_{\hat{B}}]$$

The proposed attitude determination approach is supplemented with the attitude control algorithm.

V. Magnetic Control Algorithm

Consider the Lyapunov-based control

$$\boldsymbol{m} = -k_{\omega}\boldsymbol{B}\times\boldsymbol{\Omega} - k_a\boldsymbol{B}\times\boldsymbol{S} \tag{7}$$

where $\boldsymbol{S} = (a_{23} - a_{32}, a_{31} - a_{13}, a_{12} - a_{21})$, k_a, k_{ω} are the control parameters. This is the common approach when magnetorquers implement the Lyapunov control part that is perpendicular to the geomagnetic induction vector. This control ensures the necessary attitude [20–22], provided that the control parameters are small enough and carefully adjusted. The adjustment is conducted in two steps. First, the equations of motion are linearized in the vicinity of the necessary attitude. These equations use the direct dipole geomagnetic field. They do not take into account any disturbances other than the gravity. The resulting linearized equations have periodic coefficients:

$$\begin{aligned}
\frac{dw_1}{du} &= -k'_{\omega}\frac{B_0^2}{A\omega_0^2}[(B_2^2 + B_3^2)w_1 - B_1B_2w_2 - B_1B_3w_3] \\
&\quad - 2k_a\frac{B_0^2}{A\omega_0^2}[-B_1B_2\alpha - B_1B_3\beta + (B_2^2 + B_3^2)\gamma] - w_3 \\
&\quad + \frac{B - C}{A}(w_2 - 4\gamma) \\
\frac{dw_2}{du} &= -k'_{\omega}\frac{B_0^2}{B\omega_0^2}[-B_1B_2w_1 + (B_1^2 + B_3^2)w_2 - B_2B_3w_3] \\
&\quad - 2k_a\frac{B_0^2}{B\omega_0^2}[(B_1^2 + B_3^2)\alpha - B_2B_3\beta - B_1B_2\gamma] + 3\frac{C - A}{B}\alpha \\
\frac{dw_3}{du} &= -k'_{\omega}\frac{B_0^2}{C\omega_0^2}[-B_1B_3w_1 - B_2B_3w_2 + (B_1^2 + B_2^2)w_3] \\
&\quad - 2k_a\frac{B_0^2}{C\omega_0^2}[-B_2B_3\alpha + (B_1^2 + B_2^2)\beta - B_1B_3\gamma] + w_1 \\
&\quad + \frac{A - B}{C}(w_1 + \beta) \\
\frac{d\alpha}{du} &= w_2, \qquad \frac{d\beta}{du} = w_3, \qquad \frac{d\gamma}{du} = w_1
\end{aligned}$$

Here, the control parameter k_{ω} is substituted with $k'_{\omega} = k_{\omega}\omega_0$, and so both control parameters have the same physical dimension; B_i are the geomagnetic induction vector components using the model presented by Eq. (3); and $w_i = \Omega_i/\omega_0$ are the dimensionless relative angular velocity components. Linearized equations introduce the derivative with respect to the argument of latitude. These equations are analyzed using the Floquet theory [23]. Figure 1 represents the characteristic multipliers in the vicinity of the stability area of the linearized equations of motion.

The satellite and its orbit parameters are as follows 1) circular orbit, altitude 400 km, inclination 51.7 deg, Earth radius 6371 km; and 2) inertia tensor $\boldsymbol{J} = \text{diag}(5\cdot10^{-3}, 6\cdot10^{-3}, 7\cdot10^{-3})$ kg $\cdot$ m^2.

Control parameters can be found from Fig. 1 only approximately. Thus, the second adjustment step is necessary. Initial equations of motion (with some additional disturbances, more complex geomagnetic field model, etc.) are modeled numerically with the control parameters close to the theoretically optimal ones. For the considered case, good control parameters are $k_{\omega} = 40/\omega_0$ N $\cdot$ m $\cdot$ s/T^2 and $k_a = 12$ N $\cdot$ m/T^2. Note that they are very close to the optimal ones according to Fig. 1.

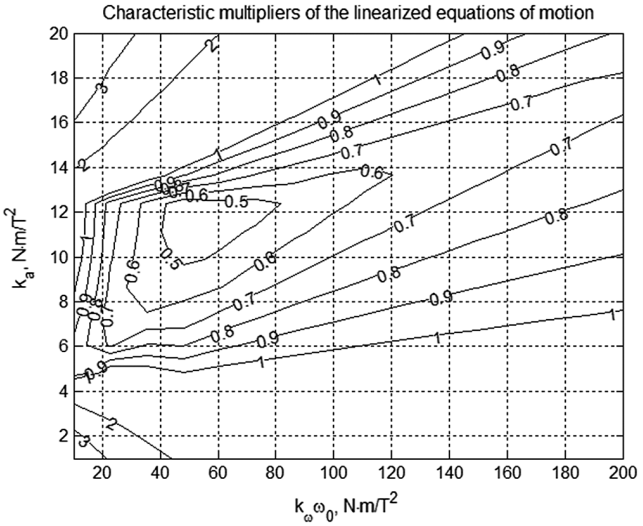

Fig. 1 Stability area.

VI. Numerical Simulation

Consider the 1U CubeSat with the orbit and mass parameters provided previously. It is equipped with three orthogonal magnetorquers with the rod diameter $d = 5.7$ mm, and so the area is $S = 10^{-4}$ m^2, the rod relative permeability is 75,000, and the number of turns is $N = 6000$ each (these parameters are similar to the magnetorquer described in [14]).

Filter initialization requires definition of the measurement errors matrix $\boldsymbol{R}$, motion equation model errors matrix $\boldsymbol{Q}$, and initial estimation errors of the state vector matrix $\boldsymbol{P}_0$.

Consider the standard measurements deviation of the induced EMF to be $\sigma_{\text{meas}} = 50$ μV. Then, the measurement errors covariance matrix is assumed to be $\boldsymbol{R} = \text{diag}(\sigma_{\text{meas}}^2, \sigma_{\text{meas}}^2, \sigma_{\text{meas}}^2)$.

The unaccounted disturbing torque is supposed to be random and of the order of $d = 5\cdot10^{-8}$ N $\cdot$ m; its distribution is Gaussian with zero mean. The model error covariance matrix is calculated using Eq. (6). Integration of Eq. (6) is rather complicated, especially for the nanosatellite onboard computer. It is reasonable to simplify this expression using the reduced and constant state transition matrix as

$$\boldsymbol{\Phi} = \begin{bmatrix} \boldsymbol{E} & \frac{1}{2}\boldsymbol{E}\Delta t \\ 0_{3\times3} & \boldsymbol{E} \end{bmatrix}$$

The matrix of the influence of the model error on the state vector is determined as

$$\boldsymbol{G} = \begin{bmatrix} 0_{3\times3} \\ \boldsymbol{J}^{-1} \end{bmatrix}$$

Then, the model errors covariance matrix is derived from Eq. (6) as follows:

$$\boldsymbol{Q} = \begin{bmatrix} \boldsymbol{E}\sigma_q^2 & \boldsymbol{E}\sigma_{\omega}\sigma_q \\ \boldsymbol{E}\sigma_{\omega}\sigma_q & \boldsymbol{E}\sigma_{\omega}^2 \end{bmatrix}, \qquad \sigma_{\omega} = I^{-1}d\Delta t, \qquad \sigma_q = I^{-1}d\Delta t^2/2$$

where I is the smallest inertia moment, Δt is the measurements sampling interval, and d is the mean-squared deviation of the disturbance torque acting on the satellite.

The initial state vector estimation is arbitrary. Suppose it to be zero (zero vector part of quaternion and zero angular velocity). Consider the maximum quaternion error $\sigma_{q_0} = 1$ and knowingly big velocity error $\sigma_{\omega_0} = 10$ deg/s. The initial error matrix is

$$\boldsymbol{P}_0 = \text{diag}(\sigma_{q_0}^2, \sigma_{q_0}^2, \sigma_{q_0}^2, \sigma_{\omega_0}^2, \sigma_{\omega_0}^2, \sigma_{\omega_0}^2)$$

Set the initial angular velocity $\boldsymbol{\omega}(t=0) = (10\omega_0, 10\omega_0, 10\omega_0)$, where the orbital angular velocity $\omega_0 = 0.06$ deg/s, and initial quaternion $\Lambda_0 = [1 \quad 0 \quad 0 \quad 0]$. The sampling measurements time is 1 s.

A. Free Motion

Figure 2 shows the free motion of the CubeSat with the specified initial conditions and parameters. The angles $\gamma_{ii} = \text{acos}(a_{ii})$ define the deviations of the body axes from the corresponding orbital axes. The satellite chaotically rotates around its center of mass. The measurements of EMF induced in the magnetorquers are presented in Fig. 3. The maximum measured value of EMF is about 0.01 V. Thus, the signal-to-noise ratio is about 200.

Consider the accuracy of the estimation of the three-axis attitude motion by the proposed algorithm. Figure 4 presents the difference between the simulated state vector and the estimated one. The accuracy of the attitude estimation after the convergence does not exceed 1 deg and 0.01 deg/s. However, one can see the time dependence of the accuracy. Particularly, near 0.75 h, the accuracy decreases for angles α and β. At that time, the output signal

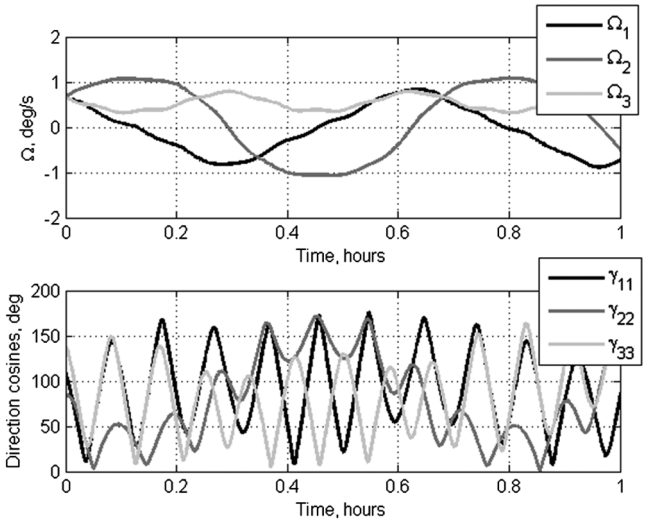

Fig. 2 Angular velocity and direction cosines during the free attitude motion of the CubeSat.

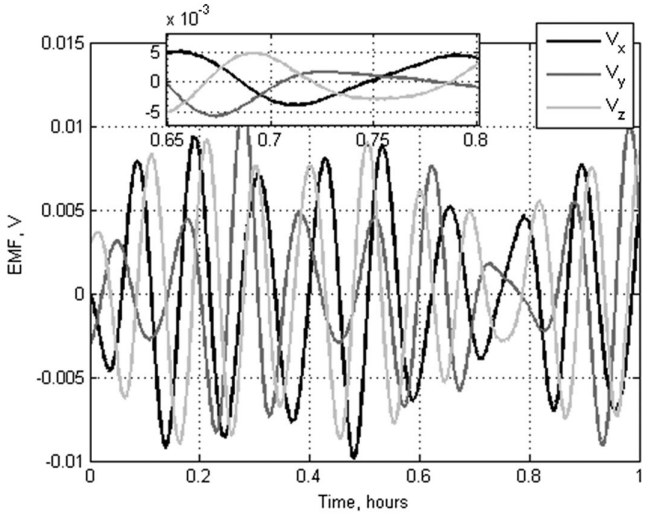

Fig. 3 Measurements of the induced EMF in the magnetorquers.

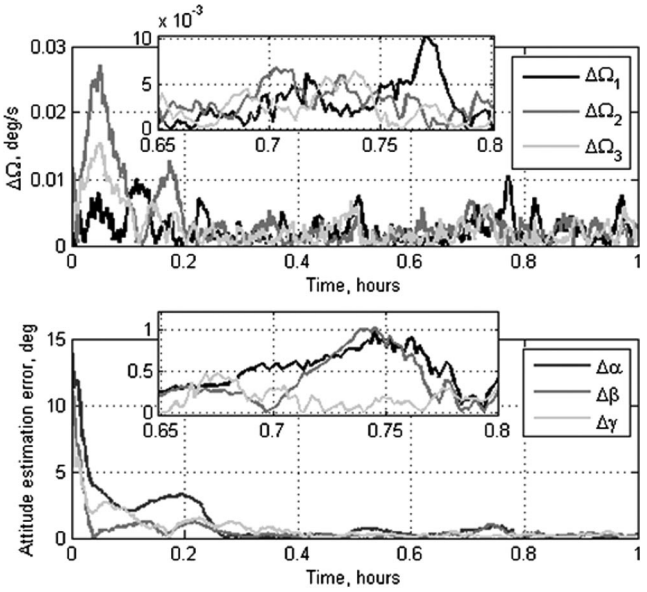

Fig. 4 Accuracy of the attitude motion estimation.

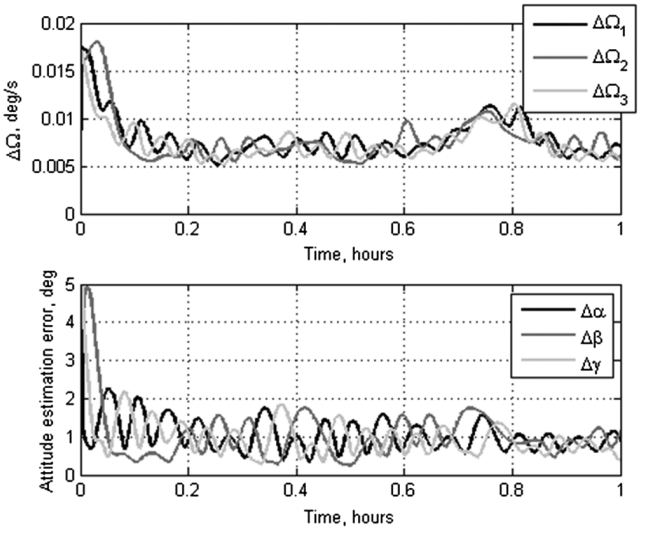

Fig. 5 Accuracy of the attitude motion estimation calculated using covariance matrix.

(see Fig. 3) was low for these two channels. That is why the errors in the attitude determination increased in that time interval.

It is interesting to calculate the accuracy using the covariance matrix $\boldsymbol{P}$. Its diagonal elements are the dispersions σ^2. Let us obtain the mean-squared deviation as $\sigma_i = \sqrt{p_{ii}}$, $i = 1, \ldots, 6$, where p_{ii} are the diagonal elements of the matrix $\boldsymbol{P}$. Figure 5 shows 3σ dependence on time. One can see that the mean-squared deviations of the state vector components are not stationary. Particularly, near 0.75 h, the expected 3σ error of the state vector estimation temporary increases. This corresponds to the effect that can be seen in the actual errors in Fig. 4. The specific behavior of the covariance matrix depends on the dynamics and the observability features of the system. In that particular case, at point 0.75 h, the observability slightly degrades because of the low signal value.

B. Controlled Motion

Consider the following control scheme. Because the magnetorquers are the sensors and actuators at the same time, the measurement time intervals are separated from the control intervals. During the measurement interval, the satellite attitude motion is

passive, and so the EMF induced in magnetorquers is inspired by the geomagnetic induction vector motion. The state vector estimation is used for the control magnetic dipole vector calculation according to Eq. (7). During the control time interval, the dipole vector of the magnetorquers is constant.

Figures 6 and 7 provide the attitude during the controlled motion. Figure 8 presents the corresponding EMF measurements. The measurement time interval is 1 s, and the control is implemented during 5 s interval. General attitude accuracy is better than 5 deg. It drops to 8 deg at worst. Stabilization accuracy decreases at about 2, 3.5, and 4.5 h (Fig. 6). Corresponding attitude estimation accuracy decrease can be seen in Fig. 7. Estimation accuracy decreases right after the best results in the stabilization (close-up in Fig. 6). The satellite acquires "too good" attitude, and its angular velocity becomes close to zero. As a result, EMF induced in magnetorquers decreases, leading to degraded estimation accuracy. This in turn leads to the less accurate stabilization. Then, the satellite angular velocity increases, the EMF increases, the Kalman filter converges, and the estimation accuracy rises again.

EMF measurements induced in magnetorquers are presented in Fig. 8. The signal value is about 800 μV for the stabilized satellite. Figure 9 provides the control torque values. The typical control torque is about $3 \cdot 10^{-7}$ N $\cdot$ m in the beginning and not more than 10^{-8} after the satellite is stabilized. This is even less than the value of the disturbing torque. However, the latter is normally distributed. Close up in Fig. 9 gives an insight into the measurements and control intervals.

Attitude estimation (and following stabilization) accuracy degradation intervals are random. Fifty simulations were run with the same initial conditions and with different measurement errors. The worst and mean attitude estimation and stabilization accuracies were determined after the Kalman filter convergence. Figure 10 provides the box plots for the worst estimation and stabilization examples. Half of the results are inside the box; the line inside the box indicates the mean value; and one quarter of the results lie below and one quarter above the box. Crosses indicate the values outside of 3σ deviation from the mean value (assuming that the data are normally distributed). Figure 11 provides the box plots for mean accuracies.

Figures 10 and 11 provide almost linear dependence between the attitude estimation accuracy and the measurements errors. Attitude stabilization accuracy decreases almost linearly also as the error increases. Note that measurement errors of the order of $\sigma_{\text{meas}} = 300\ \mu$V are only about two times less than the signal values. Nevertheless, the mean attitude estimation accuracy is about 3.5 deg in this case, and the mean attitude stabilization accuracy is about 13 deg.

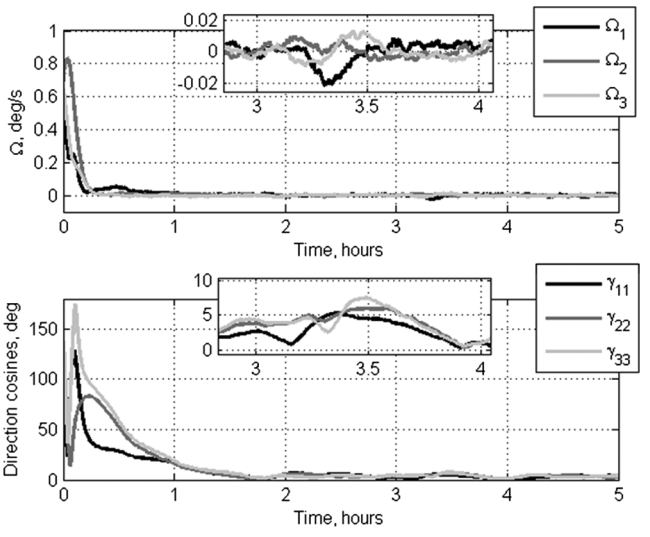

Fig. 6 Stabilization accuracy.

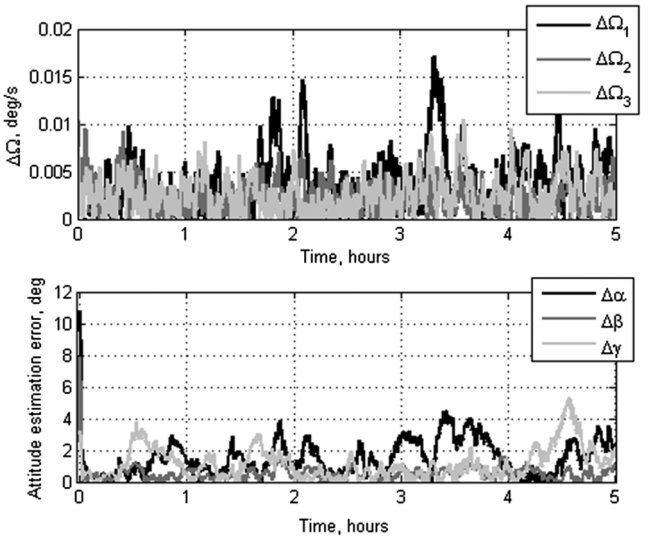

Fig. 7 Attitude estimation accuracy.

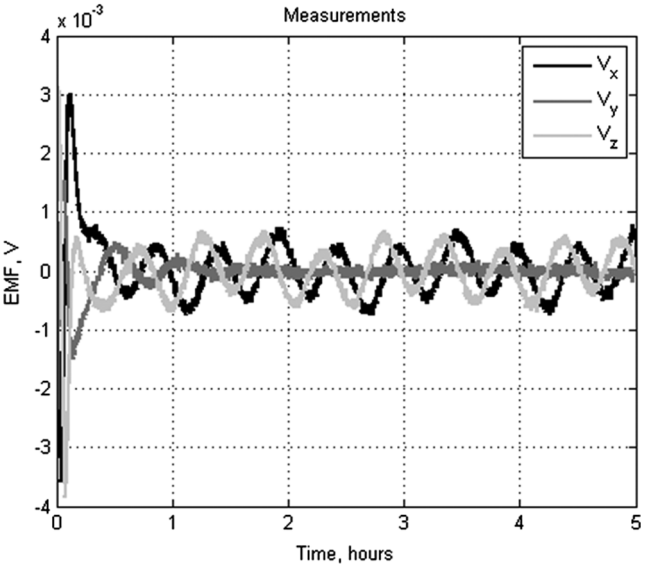

Fig. 8 Measurements of EMF during the controlled motion in case $\sigma_{\text{meas}} = 50\ \mu$V.

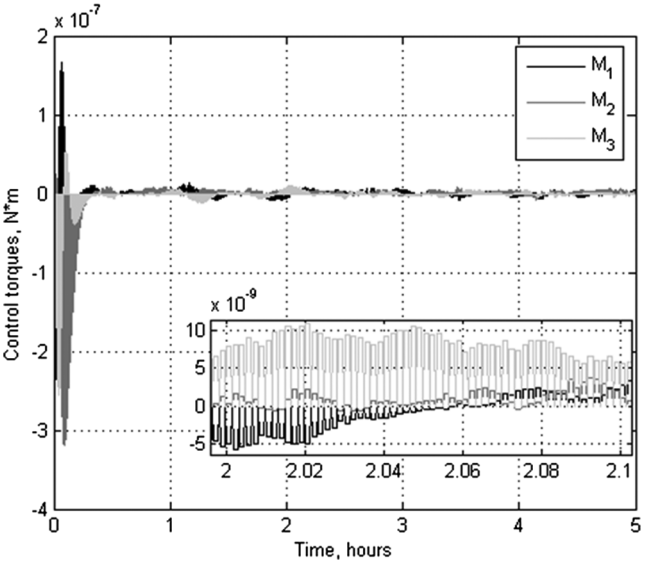

Fig. 9 Control torque values.

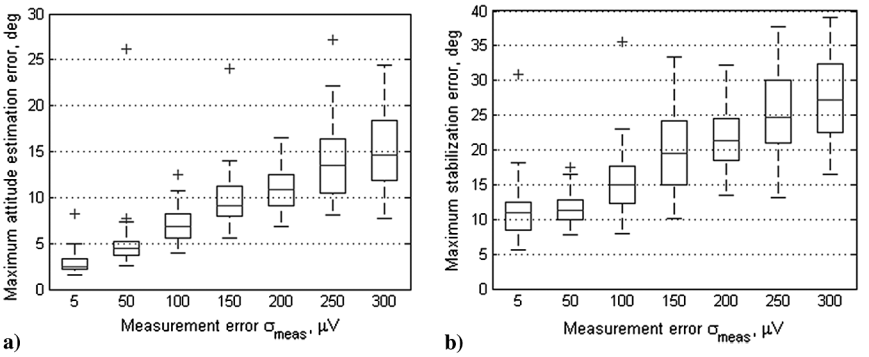

Fig. 10 Worst accuracy for a) estimation, and b) control, depending on the measurements errors.

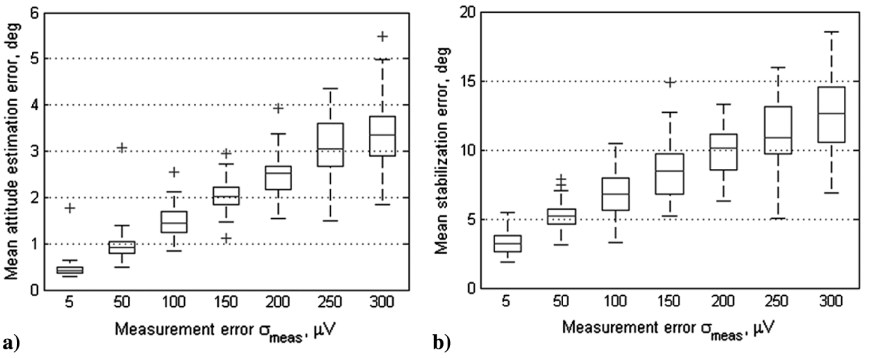

Fig. 11 Mean accuracy for a) estimation, and b) control, depending on the measurements errors.

VII. Conclusions

A satellite attitude estimation algorithm based on the measurements of the electromotive force induced in magnetorquers is proposed. The estimation accuracy strongly depends on the satellite angular velocity and measurements errors. Attitude estimation accuracy is a few degrees, whereas the stabilization accuracy with the Lyapunov control is not worse than 15 deg. This relatively low accuracy may suffice for some CubeSat missions or act as a backup measure for more demanding large spacecrafts. There is some room for improvement in future works, both on the hardware side (less noise) and the algorithm itself (for example, varying the length of the time intervals of the determination and control period).

Acknowledgments

This work is supported by the Russian Science Foundation, grant 17-71-20117.

References

[1] Springmann, J. C., Sloboda, A. J., Klesh, A. T., Bennett, M. W., and Cutler, J. W., "The Attitude Determination System of the RAX Satellite," *Acta Astronautica*, Vol. 75, June–July 2012, pp. 120–135. doi:10.1016/j.actaastro.2012.02.001

[2] Searcy, J. D., and Pernicka, H. J., "Magnetometer-Only Attitude Determination Using Novel Two-Step Kalman Filter Approach," *Journal of Guidance, Control, and Dynamics*, Vol. 35, No. 6, 2012, pp. 1693–1701. doi:10.2514/1.57344

[3] Psiaki, M. L., Martel, F., and Pal, P. K., "Three-Axis Attitude Determination via Kalman Filtering of Magnetometer Data," *Journal of Guidance, Control, and Dynamics*, Vol. 13, No. 3, 1990, pp. 506–514. doi:10.2514/3.25364

[4] Lefferts, E. J., Markley, F. L., and Shuster, M. D., "Kalman Filtering for Spacecraft Attitude Estimation," *Journal of Guidance, Control, and Dynamics*, Vol. 5, No. 5, 1982, pp. 417–429. doi:10.2514/3.56190

[5] Pittelkau, M. E., "Kalman Filtering for Spacecraft System Alignment Calibration Introduction," *Journal of Guidance, Control, and Dynamics*, Vol. 24, No. 6, 2001, pp. 1187–1195. doi:10.2514/2.4834

[6] Gai, E., Daly, K., Harrisdn, J., and Lemos, L., "Star-Sensor-Based Satellite Attitude/Attitude Rate Estimator," *Journal of Guidance, Control, and Dynamics*, Vol. 8, No. 5, 1985, pp. 560–565. doi:10.2514/3.56393

[7] Xiong, K., Liang, T., and Yongjun, L., "Multiple Model Kalman Filter for Attitude Determination of Precision Pointing Spacecraft," *Acta Astronautica*, Vol. 68, Nos. 7–8, 2011, pp. 843–852. doi:10.1016/j.actaastro.2010.08.026

[8] Abdelrahman, M., and Park, S.-Y., "Integrated Attitude Determination and Control System via Magnetic Measurements and Actuation," *Acta Astronautica*, Vol. 69, Nos. 3–4, 2011, pp. 168–185. doi:10.1016/j.actaastro.2011.03.010

[9] Ivanov, D. S., Ovchinnikov, M. Y., Penkov, V. I., Roldugin, D. S., Doronin, D. M., and Ovchinnikov, A. V., "Advanced Numerical Study of the Three-Axis Magnetic Attitude Control and Determination with Uncertainties," *Acta Astronautica*, Vol. 132, March 2017, pp. 103–110. doi:10.1016/j.actaastro.2016.11.045

[10] Tumanski, S., "Induction Coil Sensors—A Review," *Measurement Science and Technology*, Vol. 18, No. 3, 2007, pp. R31–R46. doi:10.1088/0957-0233/18/3/R01

[11] Kalman, R. E., "A New Approach to Linear Filtering and Prediction Problems," *Transactions of ASME, Series D, Journal of Basic Engineering*, Vol. 82, No. 1, 1960, pp. 35–45. doi:10.1115/1.3662552

[12] Ovchinnikov, M. Y., Penkov, V. I., Roldugin, D. S., and Pichuzhkina, A. V., "Geomagnetic Field Models for Satellite Angular Motion Studies," *Acta Astronautica*, Vol. 144, March 2018, pp. 171–180. doi:10.1016/j.actaastro.2017.12.026

[13] Tikhonov, A. A., and Petrov, K. G., "Multipole Models of the Earth's Magnetic Field," *Cosmic Research*, Vol. 40, No. 3, 2002, pp. 203–212. doi:10.1023/A:1015916718570

[14] Li, J., Post, M., Wright, T., and Lee, R., "Design of Attitude Control Systems for CubeSat-Class Nanosatellite," *Journal of Control Science and Engineering*, Vol. 2013, Dec. 2012, pp. 1–15. doi:10.1155/2013/657182

[15] Ashida, H., Fujihashi, K., Inagawa, S., Miura, Y., Omagari, K., Miyashita, N., Matunaga, S., Toizumi, T., Kataoka, J., and Kawai, N., "Design of Tokyo Tech Nano-satellite CUTE-1.7 + APDand its Operation," *Acta Astronautica*, Vol. 66, May 2010, pp. 1412–1424. doi:10.1016/j.actaastro.2009.10.035

[16] Ivanov, D. S., Ovchinnikov, M. Y., and Penkov, V. I., "Laboratory Study of Magnetic Properties of Hysteresis Rods for Attitude Control Systems of Minisatellites," *Journal of Computer and Systems Sciences International*, Vol. 52, No. 1, 2013, pp. 145–164. doi:10.1134/S1064230712060032

[17] "Analog-to-Digital Converter Design Guide High-Performance, Stand-Alone A/D Converters for a Variety of Embedded Systems Applications," Microchip Technology Inc., 2010, http://www.t-es-t.hu/download/microchip/ds21841c.pdf [retrieved 21 May 2017].

[18] Kalman, R. E., and Bucy, R. S., "New Results in Linear Filtering and Prediction Theory," *Transactions of ASME, Series D: Journal of Basic Engineering*, Vol. 83, No. 1, 1961, pp. 95–108. doi:10.1115/1.3658902

[19] Wertz, J. R., *Spacecraft Attitude Determination and Control*, Academic Press, Dordrecht, The Netherlands, 1990, Chap. 13.

[20] Ovchinnikov, M. Y., Roldugin, D. S., Ivanov, D. S., and Penkov, V. I., "Choosing Control Parameters for Three Axis Magnetic Stabilization in Orbital Frame," *Acta Astronautica*, Vol. 116, Nov.–Dec. 2015, pp. 74–77. doi:10.1016/j.actaastro.2015.06.016

[21] Ovchinnikov, M. Y., Roldugin, D. S., and Penkov, V. I., "Three-Axis Active Magnetic Attitude Control Asymptotical Study," *Acta Astronautica*, Vol. 110, May–June 2015, pp. 279–286. doi:10.1016/j.actaastro.2014.11.030

[22] Celani, F., "Robust Three-Axis Attitude Stabilization for Inertial Pointing Spacecraft Using Magnetorquers," *Acta Astronautica*, Vol. 107, Feb.–March 2015, pp. 87–96. doi:10.1016/j.actaastro.2014.11.027

[23] Malkin, I. G., *Some Problems in the Theory of Nonlinear Oscillations*, U.S. Atomic Energy Commission, Technical Information Service, Oak Ridge, TN, 1959, Chap. 3.